Acceleration and focusing of relativistic electron beams in a compact plasma device

R. Pompili [1,*] M. P. Anania,[1] A. Biagioni,[1] M. Carillo,[2] E. Chiadroni,[2] A. Cianchi,[3,4,5] G. Costa,[1] A. Curcio,[1] L. Crincoli,[1]
A. Del Dotto,[1] M. Del Giorno,[1] F. Demurtas,[3] M. Galletti,[3,4,5] A. Giribono,[1] V. Lollo,[1] M. Opromolla,[1] G. Parise,[3]
D. Pellegrini,[1] G. Di Pirro,[1] S. Romeo,[1] G. J. Silvi,[2] L. Verra,[1] F. Villa,[1] A. Zigler,[6] and M. Ferrario[1]

[1]*Laboratori Nazionali di Frascati, Via Enrico Fermi 54, 00044 Frascati, Italy*
[2]*University of Rome Sapienza, Piazzale Aldo Moro 5, 00185 Rome, Italy*
[3]*University of Rome Tor Vergata, Via della Ricerca Scientifica 1, 00133 Rome, Italy*
[4]*INFN Tor Vergata, Via della Ricerca Scientifica 1, 00133 Rome, Italy*
[5]*NAST Center, Via della Ricerca Scientifica 1, 00133 Rome, Italy*
[6]*Racah Institute of Physics, Hebrew University, 91904 Jerusalem, Israel*

Plasma wakefield acceleration represented a breakthrough in the field of particle accelerators by pushing beams to gigaelectronvolt energies within centimeter distances. The large electric fields excited by a driver pulse in the plasma can efficiently accelerate a trailing witness bunch paving the way toward the realization of laboratory-scale applications like free-electron lasers. However, while the accelerator size is tremendously reduced, upstream and downstream of it the beams are still handled with conventional magnetic optics with sizable footprints and rather long focal lengths. Here we show the operation of a compact device that integrates two active-plasma lenses with short focal lengths to assist the plasma accelerator stage. We demonstrate the focusing and energy gain of a witness bunch whose phase space is completely characterized in terms of energy and emittance. These results represent an important step toward the accelerator miniaturization and the development of next-generation table-top machines.

I. INTRODUCTION

Particle accelerators are a key engine for discoveries and started a new era providing a perspective of the microscopic world at the subatomic level [1] and subfemtosecond timescale [2]. Nevertheless, current accelerator technology based on radio frequency (RF) is limited in terms of achievable gradients and can require sizable footprints [3]. Plasma acceleration [4] represented a breakthrough and enabled the generation of tens of GV/m fields [5–8], orders of magnitude larger than RF. Many pioneering experiments demonstrated enormous accelerations of a trailing witness bunch that gained part of the energy deposited in the plasma by the driver [9–12], consisting of a high-intensity laser or charged particle beam. Considering the impressive advances that improved the overall beam quality [13,14], plasma technology has become very competitive also for user-oriented applications like free-electron lasers [15–18].

However, unlike RF accelerators, the operation of a plasma-based one requires the beams to be transversely handled both upstream and downstream of it. Indeed, the accelerated witness usually emerges from the plasma with a rather large divergence that may cause an increase of its emittance [19]. Moreover, in the case of a beam-driven plasma-wakefield accelerator (PWFA), the driver and witness bunches must be focused at the plasma entrance to transversely match the plasma [20,21]. These tasks are usually performed with conventional magnetic optics like quadrupoles or solenoids that, especially at large beam energies, can have rather long focal lengths and thus sizable footprints [22].

In this Letter, we describe a proof-of-principle experiment where we employed an innovative compact plasma-based device integrating two active-plasma lenses (APL) with a PWFA stage. We demonstrate that such a device is able to focus, accelerate, and remove the large divergence of a relativistic witness electron bunch that gains about 4.5 MeV energy over 3 cm, corresponding to an average accelerating gradient of ≈150 MV/m. The plasma is generated in each of the three modules by ionizing the Nitrogen gas here confined with a high-voltage discharge current. For this purpose the three modules are driven by their own high-voltage pulser, allowing to independently tune the discharge current and plasma density in each one. As showed in Fig. 1, the first lens focuses the driver and witness bunches at the entrance of the accelerator stage; here the driver releases its energy generating the plasma wakefield that is used to accelerate the witness bunch; finally the second lens catches both the driver and witness, in particular reducing the large divergence of the latter one to allow its transport along the beamline. In the following we show that this solution is highly tunable and provides a compact and efficient way to accelerate particles in a plasma.

II. EXPERIMENTAL SETUP

A. Generation of the driver and witness bunches

The experiment has been carried out at the SPARC_LAB facility [23] by using a 200 pC driver followed by a 50 pC
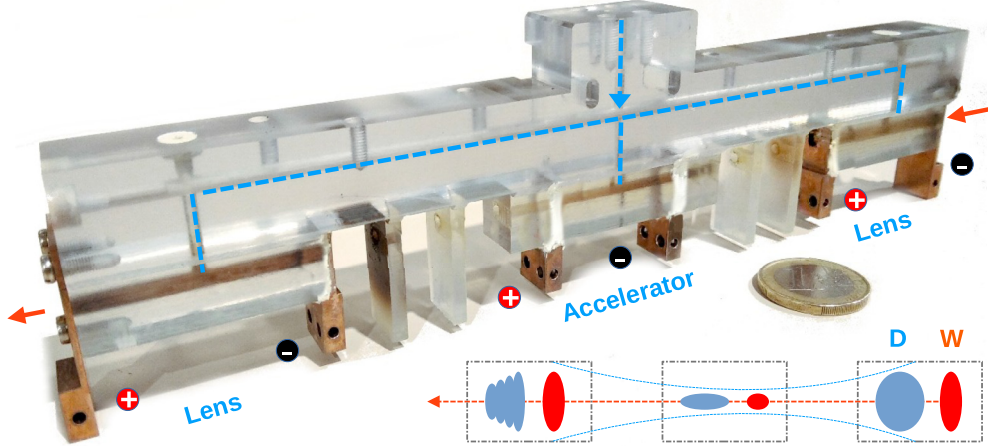
---
*riccardo.pompili@lnf.infn.it

FIG. 1. Combined capillary adopted in the experiment. The picture shows the device consisting of two active-plasma lenses and an accelerator stage. The dashed blue lines indicate the flow of Nitrogen gas that fills up the three capillaries. The plasma is produced by ionizing the gas with three independent high-voltage discharge currents applied to the three capillaries. The polarity of the discharge current on each electrode is also shown. The electron bunches propagate from right to left (red arrows). Plastic shields are located in the two drift sections to avoid electric cross-talk due to the expanding plasma plumes. The inset shows the envelopes of the driver (D) and witness (W) bunches during the propagation in each stage. The total length of the device is 19 cm; a 1€ coin is included as reference size.

witness. The bunches are generated by illuminating a copper cathode with two ultraviolet pulses [24,25] and are then accelerated by the linac, consisting of a RF gun followed by three accelerating sections. Downstream of the linac, after the temporal compression operated in the velocity-bunching regime [26], the two bunches reach final energies $E_d = 71.6 \pm 0.1$ MeV and $E_w = 71.9 \pm 0.1$ MeV with energy spreads $\sigma_{E,d} = 0.49 \pm 0.03$ MeV and $\sigma_{E,w} = 0.72 \pm 0.04$ MeV, and durations $\sigma_{t,d} = 185 \pm 39$ fs and $\sigma_{t,w} = 55 \pm 32$ fs. The witness is temporally delayed with respect to the driver by $\Delta t = 1.15 \pm 0.03$ ps. The normalized vertical emittances of the two bunches are $\varepsilon_{n,d} = 6.2 \pm 0.7$ μm and $\varepsilon_{n,w} = 4.8 \pm 0.4$ μm. The beam diagnostics consists of a cerium-doped yttrium aluminum perovskite (Ce:YAP) scintillating screen located 5 cm downstream from the plasma device to measure the beam transverse profile. A magnetic spectrometer is then used to characterize the energy profiles of the bunches.

B. Combined capillary of the PWFA and APL stages

The plasma device consists of a Lexan polycarbonate capillary with 19 cm total length and 2 mm hole diameter. It is installed in a vacuum chamber directly connected with a windowless, three-stage differential pumping system that ensures 10^{-8} mbar pressure in the RF linac while flowing the gas. This solution allows to transport the beam without encountering any window, thus not degrading its emittance by multiple scattering. As showed in Fig. 1, the three plasma stages are 3 cm-long and have two copper-tungsten electrodes attached at their ends where the high-voltage discharge is applied. $f \approx 5$ cm being the focal length expected for each APL, two 5 cm long open drift sections are located between the PWFA module and the two APLs, i.e., the same distance between the end of the second APL and the Ce:YAP screen. A high-speed solenoid valve is used to fill the three capillaries with nitrogen gas by means of a common rail located above them. Two shields with 2 mm hole diameter are inserted in

the two open drift sections to avoid the plasma jets emitted by each stage to reach the closer one. The high-voltage discharge currents are provided by three pulsers consisting of several capacitor banks able to generate up to 1.6 kA peak current when charged at 20 kV. The trigger timing of each pulser is independently controlled allowing to tune the discharge currents and, consequently, the plasma densities experienced by the electron beam in each of the three plasma stages. The stabilization of the discharge process and plasma formation is obtained by preionizing the gas with a Nd:YAG laser that reduced the discharge timing jitter down to few nanoseconds [27,28]. The laser is installed close to the capillary vacuum chamber and is injected into it by means of a metallic mirror.

III. EXPERIMENTAL RESULTS

To demonstrate the acceleration and focusing provided by this device we transported the driver and witness bunches up to the entrance of the first APL. The maximum focusing with the APLs is obtained by setting the beam time of arrival in correspondence of the discharge current peak; at this time the resulting plasma densities in the APLs are $n_p \approx 2 \times 10^{17}$ cm^{-3}, measured by means of a Stark-broadening diagnostics [29]. Conversely, to reach a plasma density $n_p \approx 4 \times 10^{15}$ cm^{-3} in the PWFA stage optimized for the driver-witness configuration described so far and used in previous experiments [13,16], its discharge current is triggered ≈ 8 μs in advance so that it lowers down due to plasma recombination [30]. The resulting configuration is reported in Fig. 2 with the discharge current set to $I_{PWFA} \approx 250$ A on the PWFA stage, $I_{APL,1} \approx 620$ A on the first APL, and $I_{APL,2} \approx 670$ A on the second one. The optimal parameters of the two APLs in terms of discharge current and timing are obtained by measuring the beam on the Ce:YAP screen with only the second lens turned on (the first one and the PWFA are turned off). Indeed, being the distance between two APLs and the PWFA stage the same between the screen and the second lens, we set up
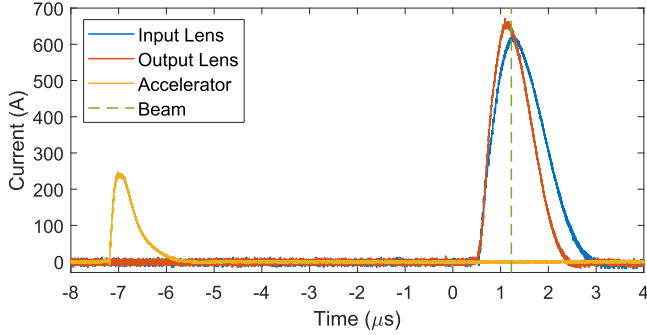
FIG. 2. Discharge current pulses. The accelerator stage (yellow) is triggered ≈ 8 μs before the electron beam (dashed green line) so that the plasma density reaches the desired value n_p during the recombination. Conversely, the two active-plasma lenses (red and blue lines) are turned on a few hundreds of ns before so that they experience the strongest focusing in correspondence of the current peak.

the latter one to produce a beam waist on the screen and then applied the same discharge timing to the first lens. We also set $I_{APL,2} \gtrsim I_{APL,1}$ to take into account the increase of the witness energy downstream of the PWFA.

Figure 3 shows a scan of the beam spot size performed on the screen by varying the trigger timing of the second APL current discharge with respect to the beam time of arrival. As previously said, the first APL and the PWFA stage are turned off on purpose. The values are computed from images with both bunches present, thus they represent a convolution of the two transverse profiles. Indeed, in the velocity-bunching regime the two bunches are generated together from the photocathode and then temporally compressed in the first accelerating section downstream of the RF gun. Here the
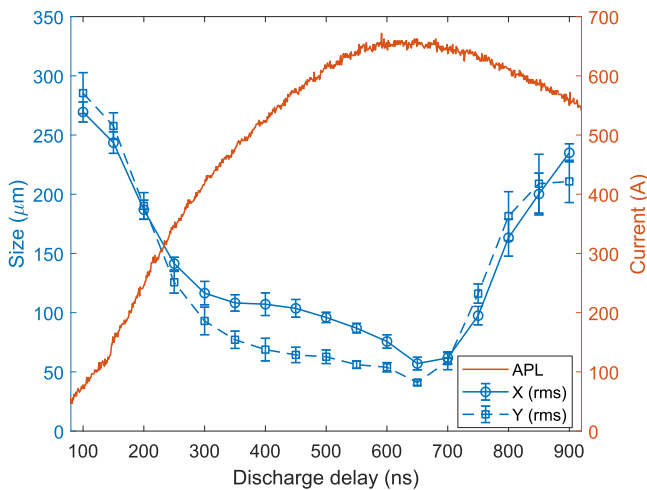

FIG. 3. Active-plasma lens scan. The data points (blue) show the horizontal (X) and vertical (Y) beam sizes measured on the screen downstream of the capillary. The scan is achieved by turning on only the second lens while delaying its discharge current with respect to the beam time of arrival. The errorbars are obtained as the standard deviations of the 50 shots collected for each delay. The corresponding discharge current (red) is shown on the right axis.
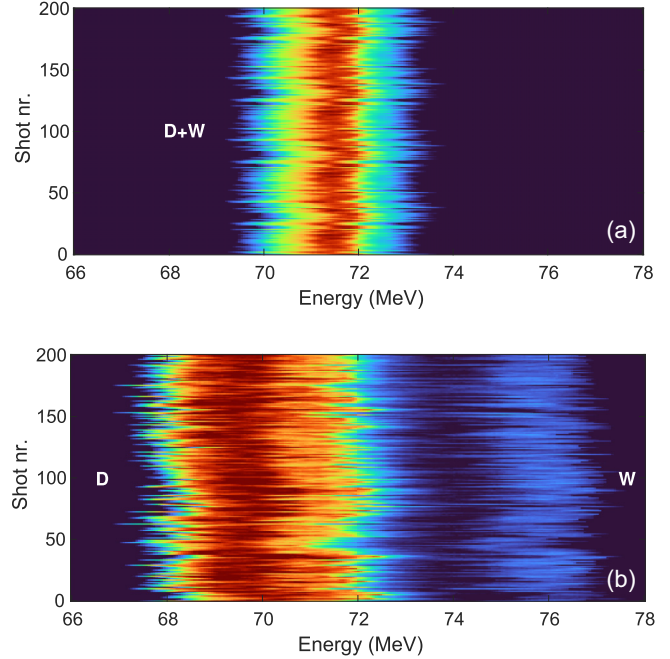

FIG. 4. Energy spectra with the accelerator stage turned off and on. The plots report the energy spectra of 200 consecutive acquisitions of the driver (D) and witness (W) beams. Each plot is obtained with the active-plasma lenses turned on and with the accelerator stage turned off (a) and on (b). The spectra are obtained in correspondence of the scintillator screen located downstream of the magnetic spectrometer.

bunches cross each other, swapping their positions so that the witness, which was photoemitted before the driver, is moved behind it [26]. Therefore it is not possible to measure the single bunch profile by simply blocking the other one on the photocathode since this would affect the entire bunch dynamics. One can see that when the beam is beforehand with respect to the discharge trigger (i.e., the plasma has not yet been created), its spot size is $\sigma_{x(y)} = 336(274) \pm 18(11)$ μm. Then, by delaying it with respect to the discharge current, the beam is gradually focused down to a waist size $\sigma_{x(y)} = 57(41) \pm 5(2)$ μm at ≈ 650 ns. Considering that such a waist is given by $\sigma = \sqrt{\beta \varepsilon_n / \gamma}$ with $\beta = f^2/\beta_i \approx 5.3$ mm, the Twiss β function at waist location [31], $\beta_i = 0.47 \pm 0.06$ m the corresponding value at APL entrance, and γ the relativistic Lorentz factor, to explain the experimentally obtained value one has to assume that the normalized emittance increased up to $\varepsilon_n \approx 30$ μm during the focusing operated by the APL. This aspect will be discussed in the following with the support of numerical simulations.

After turning on the PWFA with the second APL and setting their discharge timings as reported in Fig. 2, we proceeded with the experiment by measuring the witness energy gain on the scintillating screen located downstream of the magnetic spectrometer. Figure 4(a) shows 200 consecutive energy spectra of the two bunches with the PWFA stage turned off. Once turned on, see Fig. 4(b), clear signatures of witness acceleration are found. Its final energy is $E_w = 76.35 \pm 0.27$ MeV, corresponding to a ≈ 150 MV/m accelerating gradient, with a resulting energy spread $\sigma_{E,w} = 1.09 \pm 0.12$ MeV.

The normalized emittance of the accelerated witness is evaluated on the same screen downstream of the magnetic spectrometer where the two bunches are well separated in energy. Several methods can be employed to retrieve the normalized emittance. Previous experiments, for instance, estimated the emittance in a single-shot way by sampling the vertical size of the beam as a function of the energy [32,33]. Such a technique, however, requires rather large energy spreads ($\gg 1\%$) and are thus not applicable to our case and, in general, to low energy spread beams. Therefore, considering also the high stability of the accelerated witness in terms of energy jitter ($\approx 0.3\%$), we employed the classical quadrupole scan technique to estimate its vertical emittance [34]. The scan is obtained by measuring the witness vertical spot size as a function of the current used in the electromagnetic quadrupoles located between the capillary exit and the screen. By performing a numerical fit on the experimental values we obtain a normalized emittance $\varepsilon_{n,w} = 12.6 \pm 1.1$ μm for the plasma accelerated witness.

IV. NUMERICAL SIMULATIONS

To support the experimental results we performed a complete start-to-end simulation where we studied the interaction of the two bunches with the plasma background. The bunches are set to reproduce the experimental ones at the capillary entrance with initial spot sizes $\sigma_{r,d} \approx 330$ μm and $\sigma_{r,w} \approx 190$ μm, estimated by performing a back tracking from the location where the emittance is measured [35]. The focusing produced by the APLs is computed with a one-dimensional analytical model that takes into account the radial plasma temperature profile to retrieve the current density $J_D(r)$ flowing in the capillary and, in turn, the induced magnetic field as $B_{APL}(r) = \mu_0/r \cdot \int_0^r J_D(r')r'dr'$ [36,37]. Figure 5(a) shows a snapshot of the two bunches propagating in the plasma background of the PWFA stage. The horizontal and vertical axes represent the comoving longitudinal (ξ) and radial (r) coordinates. The interaction with the plasma is in the quasi-nonlinear (QNL) regime, where the driver density exceeds the plasma one and induces blowout but, due to its relatively small charge, the produced perturbation is linear [38]. The witness is located in the positively charged region produced by the driver and it is consequently accelerated. The evolution of the driver and witness spot sizes and normalized emittances along all the three plasma stages is reported in Fig. 5(b). As expected, the emittances grow along the first APL, especially the driver one that reaches $\varepsilon_{n,d} \approx 33$ μm in agreement with the previous considerations. A similar behavior is noticeable also in the second lens highlighting that the focusing is nonlinear [37] and its effects are more evident on the driver bunch due to its larger spot size at the APL entrance [39]. In this case $\approx 3\%$ of driver particles are lost at the entrance of the PWFA, as highlighted by the slight decrease of its emittance at $z \approx 9$ cm, while no witness particle is lost along the propagation.

A. Emittance increase and further steps toward its optimization

For the witness, the major increase of emittance is reached along the PWFA stage and indicates a transverse mismatch of its spot size similarly to what observed in a previous
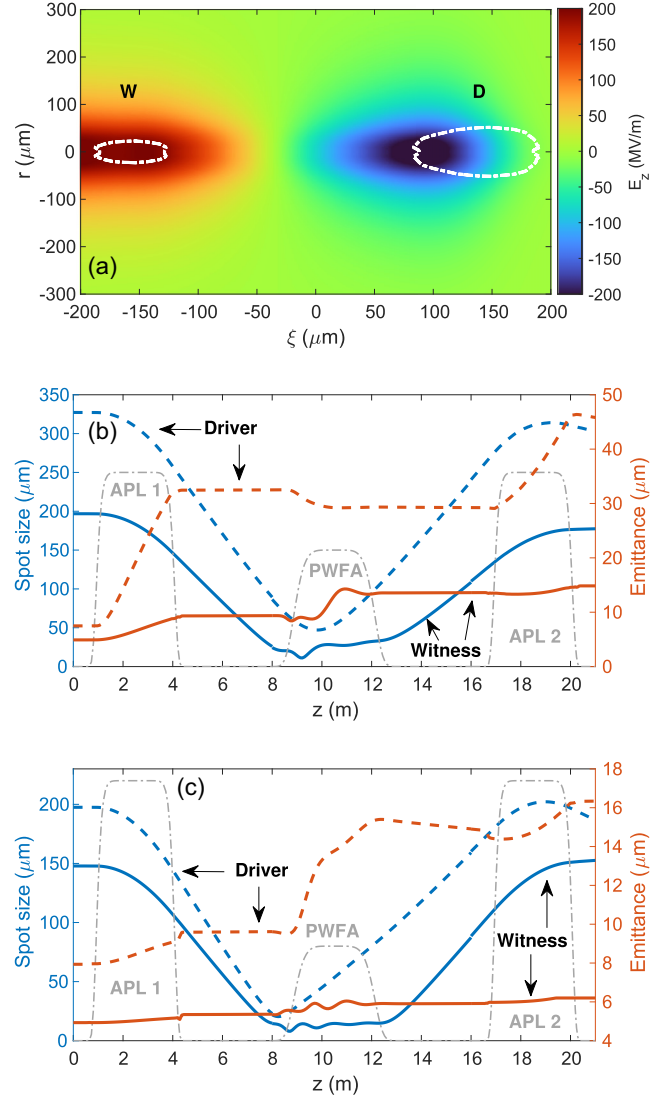

FIG. 5. Start-to-end simulations of the driver-witness evolution along the three plasma stages. (a) Accelerating field (E_z) generated in the PWFA stage. The positions of the driver (D) and witness (W) bunches are represented by the dashed lines. (b) Spot size and normalized emittance of the witness (solid) and driver (dashed). The three plasma stages are represented with gray dotted dashed lines. (c) Optimized configuration employing smaller spot sizes at the entrance.

experiment [34]. Downstream of the second APL its emittance is $\varepsilon_{n,w} \approx 14$ μm, in good agreement with the experimental one. These results point out that the performances of the overall device can be improved by properly optimizing the bunch spot sizes at the entrance of the APLs. It is well known that the interaction with plasma generates beam-driven wakefields that can strongly affect the bunch dynamics [40]. In this context, passive plasma lenses have been widely investigated [41,42] and are able to produce a net beam focusing through the plasma neutralization of the space-charge fields. In our specific case we refer to the so-called overdense passive lenses where $n_b \ll n_p$, with n_b indicating the bunch density. When dealing with active plasma lenses we therefore have to consider their combined effect [43]. The nonlinearities of the

overall focusing can be minimized by manipulating both the bunch shape and the capillary-discharge setup. The strength of the radial plasma wakefield is governed both by n_b and n_p [44] and its effect can be reduced by decreasing both, i.e., by operating with low plasma densities or by entering into the plasma with a large transverse spot (corresponding to a lower n_b [45]). On the contrary, the linearity of the APL field is guaranteed only at small radii. It implies that small transverse spots are in this case preferable. In such a way the beam tails would not reach the nonlinear region of the APL magnetic field located at large radii. This guarantees a smaller emittance deterioration and, in turn, a smaller beam waist at the PWFA. Figure 5(c) shows the same start-to-end simulation obtained by setting smaller spot sizes at the entrance of the first APL, in this case $\sigma_{r,d} \approx 200$ μm and $\sigma_{r,w} \approx 150$ μm. Considering the larger bunch densities that correspond to the smaller spot sizes, the plasma density in the two APLs is increased to $n_p = 2 \times 10^{18}$ cm^{-3} to avoid the generation of transverse plasma wakefields that may further deteriorate the emittance [39]. As a result the resulting emittance is $\varepsilon_{n,w} \approx 6.1$ μm, corresponding to a $\approx 20\%$ growth.

V. CONCLUSIONS

In conclusion, we reported a proof-of-principle experiment where three plasma stages have been merged in a compact device able to achieve the focusing, acceleration, and extraction of a witness bunch in a plasma-based accelerator. The results demonstrate the feasibility of such an approach and allowed an energy gain of ≈ 4.5 MeV over a distance of 3 cm. The integration of the two active-plasma lenses enabled the realization of short focal lengths (≈ 5 cm) making the entire device very compact. The experiment represents a first attempt toward the accelerator system miniaturization, suggesting a simple and affordable solution in terms of sizes and costs toward the development ultracompact next-generation accelerators.

The data that support the findings of this study are available from the corresponding author on reasonable request.

[1] H. Yoneda *et al.*, Nature (London) **524**, 446 (2015).

[2] P. K. Maroju *et al.*, Nature (London) **578**, 386 (2020).

[3] T. Argyropoulos, N. Catalan-Lasheras, A. Grudiev, G. Mcmonagle, E. Rodriguez-Castro, I. Syrachev, R. Wegner, B. Woolley, W. Wuensch, H. Zha, V. Dolgashev, G. Bowden, A. Haase, T. G. Lucas, M. Volpi, D. Esperante-Pereira, and R. Rajamaki, Phys. Rev. Accel. Beams **21**, 061001 (2018).

[4] T. Tajima and J. M. Dawson, Phys. Rev. Lett. **43**, 267 (1979).

[5] S. P. Mangles *et al.*, Nature (London) **431**, 535 (2004).

[6] J. Faure, Y. Glinec, A. Pukhov, S. Kiselev *et al.*, Nature (London) **431**, 541 (2004).

[7] I. Blumenfeld *et al.*, Nature (London) **445**, 741 (2007).

[8] A. J. Gonsalves, K. Nakamura, J. Daniels, C. Benedetti, C. Pieronek, T. C. H. de Raadt, S. Steinke, J. H. Bin, S. S. Bulanov, J. van Tilborg, C. G. R. Geddes, C. B. Schroeder, C. Toth, E. Esarey, K. Swanson, L. Fan-Chiang, G. Bagdasarov, N. Bobrova, V. Gasilov, G. Korn, P. Sasorov, and W. P. Leemans, Phys. Rev. Lett. **122**, 084801 (2019).

[9] V. Malka *et al.*, Science **298**, 1596 (2002).

[10] M. Litos *et al.*, Nature (London) **515**, 92 (2014).

[11] S. Steinke *et al.*, Nature (London) **530**, 190 (2016).

[12] E. Adli *et al.*, Nature (London) **561**, 363 (2018).

[13] R. Pompili *et al.*, Nat. Phys. **17**, 499 (2021).

[14] C. A. Lindstrom, J. M. Garland, S. Schroder, L. Boulton, G. Boyle, J. Chappell, R. DArcy, P. Gonzalez, A. Knetsch, V. Libov, G. Loisch, A. MartinezdelaOssa, P. Niknejadi, K. Poder, L. Schaper, B. Schmidt, B. Sheeran, S. Wesch, J. Wood, and J. Osterhoff, Phys. Rev. Lett. **126**, 014801 (2021).

[15] W. Wang *et al.*, Nature (London) **595**, 516 (2021).

[16] R. Pompili *et al.*, Nature (London) **605**, 659 (2022).

[17] M. Galletti *et al.*, Phys. Rev. Lett. **129**, 234801 (2022).

[18] M. Labat *et al.*, Nat. Photonics **17**, 150 (2023).

[19] M. Migliorati *et al.*, Phys. Rev. Spec. Top.–Accel. Beams **16**, 011302 (2013).

[20] P. Muggli, B. E. Blue, C. E. Clayton, S. Deng, F. J. Decker, M. J. Hogan, C. Huang, R. Iverson, C. Joshi, T. C. Katsouleas, S. Lee, W. Lu, K. A. Marsh, W. B. Mori, C. L. OConnell, P. Raimondi, R. Siemann, and D. Walz, Phys. Rev. Lett. **93**, 014802 (2004).

[21] R. Ariniello, C. E. Doss, K. Hunt-Stone, J. R. Cary, and M. D. Litos, Phys. Rev. Accel. Beams **22**, 041304 (2019).

[22] G. White *et al.*, J. Instrum. **17**, P05042 (2022).

[23] M. Ferrario *et al.*, Nucl. Instrum. Methods Phys. Res., Sect. B **309**, 183 (2013).

[24] M. Ferrario *et al.*, Nucl. Instrum. Methods Phys. Res., Sect. A **637**, S43 (2011).

[25] R. Pompili *et al.*, Opt. Lett. **46**, 2844 (2021).

[26] R. Pompili *et al.*, Nucl. Instrum. Methods Phys. Res., Sect. A **829**, 17 (2016).

[27] A. Biagioni *et al.*, Plasma Phys. Controlled Fusion **63**, 115013 (2021).

[28] M. Galletti *et al.*, Symmetry **14**, 450 (2022).

[29] A. Biagioni *et al.*, J. Instrum. **14**, C03002 (2019).

[30] S. Romeo *et al.*, AIP Adv. **11**, 065217 (2021).

[31] R. Pompili *et al.*, Rev. Sci. Instrum. **89**, 033302 (2018).

[32] R. Weingartner *et al.*, Phys. Rev. Spec. Top.–Accel. Beams **15**, 111302 (2012).

[33] S. Barber *et al.*, Plasma Phys. Controlled Fusion **60**, 054015 (2018).

[34] V. Shpakov, M. P. Anania, M. Behtouei, M. Bellaveglia, A. Biagioni, M. Cesarini, E. Chiadroni, A. Cianchi, G. Costa, M. Croia, A. DelDotto, M. Diomede, F. Dipace, M. Ferrario, M. Galletti, A. Giribono, A. Liedl, V. Lollo, L. Magnisi, A. Mostacci, G. DiPirro, L. Piersanti, R. Pompili, S. Romeo, A. R. Rossi, J. Scifo, C. Vaccarezza, F. Villa, and A. Zigler, Phys. Rev. Accel. Beams **24**, 051301 (2021).

[35] Y. Yang *et al.*, Rev. Sci. Instrum. **85**, 2 (2014).

[36] N. A. Bobrova, A. A. Esaulov, J.-I. Sakai, P. V. Sasorov, D. J. Spence, A. Butler, S. M. Hooker, and S. V. Bulanov, Phys. Rev. E **65**, 016407 (2001).

[37] R. Pompili *et al.*, Appl. Phys. Lett. **110**, 104101 (2017).

[38] J. B. Rosenzweig *et al.*, AIP Conf. Proc. **1299**, 500 (2010).

[39] R. Pompili, M. P. Anania, M. Bellaveglia, A. Biagioni, S. Bini, F. Bisesto, E. Brentegani, F. Cardelli, G. Castorina, E. Chiadroni, A. Cianchi, O. Coiro, G. Costa, M. Croia, D. DiGiovenale, M. Ferrario, F. Filippi, A. Giribono, V. Lollo, A. Marocchino, M. Marongiu, V. Martinelli, A. Mostacci, D. Pellegrini, L. Piersanti, G. DiPirro, S. Romeo, A. R. Rossi,

J. Scifo, V. Shpakov, A. Stella, C. Vaccarezza, F. Villa, and A. Zigler, Phys. Rev. Lett. **121**, 174801 (2018).

[40] R. Govil, W. P. Leemans, E. Y. Backhaus, and J. S. Wurtele, Phys. Rev. Lett. **83**, 3202 (1999).

[41] J. J. Su, T. Katsouleas, J. M. Dawson, and R. Fedele, Phys. Rev. A **41**, 3321 (1990).

[42] G. Hairapetian, P. Davis, C. E. Clayton, C. Joshi, S. C. Hartman, C. Pellegrini, and T. Katsouleas, Phys. Rev. Lett. **72**, 2403 (1994).

[43] A. Marocchino, M. P. Anania, M. Bellaveglia, A. Biagioni, S. Bini, F. Bisesto, E. Brentegani, E. Chiadroni, A. Cianchi, M. Croia, D. D. Giovenale, M. Ferrario, F. Filippi, A. Giribono, V. Lollo, M. Marongiu, A. Mostacci, G. D. Pirro, R. Pompili, S. Romeo *et al.*, Appl. Phys. Lett. **111**, 184101 (2017).

[44] P. Chen, J. Su, T. Katsouleas, S. Wilks, and J. Dawson, IEEE Trans. Plasma Sci. **15**, 218 (1987).

[45] J. van Tilborg, S. Barber, C. Benedetti, C. Schroeder, F. Isono, H.-E. Tsai, C. Geddes, and W. Leemans, Phys. Plasmas **25**, 056702 (2018).